Chemical Bonding, Electron Affinity, and Ionization Energies of the Homonuclear 3d Metal Dimers

Gennady L. Gutsev* and Charles W. Bauschlicher, Jr.†

NASA Ames Research Center, Moffett Field, California 94035

Received: January 31, 2003; In Final Form: March 31, 2003

Electronic and geometrical structures of the homonuclear 3d metal dimers M_2 (from Sc_2 to Zn_2) as well as their M_2^- anions and M_2^+ cations are computed using density functional theory with six generalized gradient approximations for the exchange-correlation potential. The neutral ground states are assigned as follows: Sc_2 ($^5\Sigma_u^-$), Ti_2 ($^3\Delta_g$), V_2 ($^3\Sigma_g^-$), Cr_2 ($^1\Sigma^+$), Mn_2 ($^{11}\Pi_u$), Fe_2 ($^7\Delta_u$), Co_2 ($^5\Delta_g$), Ni_2 ($^3\Sigma_g^-$), Cu_2 ($^1\Sigma_g^+$), and Zn_2 ($^1\Sigma_g^+$). The anions are assigned as follows: Sc_2^- ($^4\Sigma_g^-$), Ti_2^- ($^4\Delta_u$), V_2^- ($^4\Sigma_u^-$), Cr_2^- ($^2\Sigma^+$), Mn_2^- ($^{10}\Sigma_g^-$), Fe_2^- ($^8\Delta_g$), Co_2^- ($^6\Delta_u$), Ni_2^- ($^4\Sigma_u^-$), and Cu_2^- ($^2\Sigma_u^+$) (Zn_2^- is unbound). The cations ground states are: Sc_2^+ ($^4\Sigma_g^-$), Ti_2^+ ($^2\Delta_g$), V_2^+ ($^4\Sigma_g^-$), Cr_2^+ ($^2\Sigma^+$), Mn_2^+ ($^{10}\Pi_u$), Fe_2^+ ($^8\Delta_u$), Co_2^+ ($^6\Gamma_g$), Ni_2^+ ($^4\Delta_g$), Cu_2^+ ($^2\Sigma_g^+$), and Zn_2^+ ($^2\Sigma_u^+$). A natural bond (NBO) analysis is used to obtain the chemical bonding patterns in the neutral and charged dimers. The results of the NBO analysis allow us to explain the changes in the ground-state spin multiplicities and spatial symmetries when moving along the neutral and ionic series. Consistent changes in the chemical bonding patterns of the neutral and charged dimers lend further support to our assignment of the ground states in the M_2^- and M_2^+ series. Our calculated adiabatic electron affinities and ionization energies are in good agreement with experiment.

I. Introduction

Homonuclear 3d metal dimers have proved to be difficult for both experimental[1] and theoretical[2] studies. Given the complexity of the dimer calculations, it is clear that only density functional theory (DFT) can be used for the study of larger metal clusters. Therefore it is very useful to calibrate DFT for the metal dimers, where there is a sizable quantity of highly accurate experimental data and some results obtained using high levels of theory. Recently two DFT studies[3,4] were performed for the neutral dimers from Sc_2 to Cu_2 using different methods, and no consensus was achieved in assigning the ground states of Mn_2 and Ni_2. For Mn_2, there is a dilemma: is its ground state $^1\Sigma_g^+$ or does it have a spin multiplicity of eleven[3] ($^{11}\Sigma_u^+$ or $^{11}\Pi_u$)? For Ni_2, it is unclear if its ground state is a singlet or a triplet and what spatial symmetry it possesses. While Hirao and co-workers[3] have considered only triplet states of Ni_2, Schaefer and co-workers[4] considered only singlet states. In addition to the problems with Ni_2 and Mn_2, both of these studies (as well as the majority of previous studies cited elsewhere[1−4]) assign the ground state of Cr_2 as $^1\Sigma_g^+$, but the disagreement with experiment is so large that one might question if the theory and experiment refer to the same state. As was found in both papers,[3,4] pure density functional theory (DFT) methods perform better than hybrid DFT or many-body perturbation methods. Schaefer and co-workers[4] concluded "... it appears that DFT paints a surprisingly plausible picture of these metal diatomics."

We are unaware of any systematic studies for either the anions or the cations of the homonuclear 3d metal dimers. While no systematic study exists, there are some theoretical and experimental data available for both the anions and cations. Among the anions, the spectroscopic data were derived from laser photoelectron spectra for Cr_2^-,[5] Fe_2^-,[6,7] Co_2^-,[8] Ni_2^-,[8] and Cu_2^-.[9] Correspondingly, the adiabatic electron affinities (EA_{ad}) of their neutral parents were determined.

For the M_2^+ cations, the spectroscopic data of several of them were obtained by different methods. Knight et al.[10] have assigned $^4\Sigma^-$ as the ground state of Sc_2^+ from their ESR spectra of the cations trapped into neon matrices. The ground state of V_2^+ was also assigned[11] as $^4\Sigma^-$ by using resonant two photon ionization (R2PI) spectroscopy. The equilibrium bond distances of V_2^+ and Ni_2^+ were obtained from zero-electron kinetic energy photoelectron[12] and rotationally resolved photodissociation spectra,[13] respectively. From ESR experiments, van Zee and Weltner[14] concluded that the ground state of Mn_2^+ is $^{12}\Sigma$, which was recently confirmed[15] by the results of photodissociation spectroscopy. The R2PI study[16] has assigned the ground state of Cu_2^+ as $^2\Sigma_g^+$. The ionization energies were obtained[11,16−19,25,27,28] for all the dimers except Sc_2 and Ti_2. Experimental dissociation energies are available[20−28] for all the M_2^+ cations except Sc_2^+.

Previous DFT computations have been performed for Sc_2^-,[29] Cr_2^-,[30] Mn_2^-,[30] Fe_2^-,[31−33] Co_2^-,[34] Ni_2^-,[35,36] and Cu_2^-.[37] While the ground-state spin multiplicities were reported, the spatial symmetry of the ground state was not reported for Cr_2^-, Mn_2^-, and Ni_2^-. A few ab initio studies have been performed so far on Fe_2^-[7,39−41] and Cu_2^-.[42,43]

Recent DFT calculations confirmed[44] that the ground state of V_2^+ is $^4\Sigma_g^-$, and the computed bond length of 1.756 Å is in close agreement with the experimental value[12] of 1.735 Å. In accord with experiment,[14] both DFT[45,46] and ab initio[47] studies have predicted the ground state of Mn_2^+ to be $^{12}\Sigma_g^+$. The Ni_2^+ cation was the subject of at least two ab initio studies[48,49] in which its ground state was found to be $^4\Sigma_g^+$[48] and $^4\Sigma_u^-$.[49] In

* Corresponding author. ELORET Corp., Mail Stop 230-3. E-mail: ggutsev@mail.arc.nasa.gov

† Space Technology Division, Mail Stop 230-3.

10.1021/jp030146v CCC: $25.00
Published on Web 05/15/2003

agreement with experiment, Partridge et al.[50] found the ground state of Cu_2^+ to be $^2\Sigma_g^+$.

The aim of this paper is fourfold: (a) to asset the performance of several of the most popular DFT functionals for both neutral and singly charged homonuclear 3d metal dimers by comparison of the results obtained to the experimental data; (b) to assign those states of the homonuclear 3d metal dimer ions which are unavailable from experimental or reliable theoretical sources; (c) to confirm our assignment by consistency between the results of the natural bond (NBO) analysis for the neutral and charged dimers, as this analysis provides a qualitative description of changes in the electronic structure of a species due to attachment or detachment of an electron; (d) to explain on the basis of the NBO analysis why the spin multiplicities of the neutral dimers do not seem to have a simple correlation with the spin multiplicities of their constituent atoms. This would allow us to gain insight in the spin multiplicity changes when moving from Sc_2 to Zn_2.

II. Computational Details

Our calculations were performed using the Gaussian98 program.[51] The standard (15s11p6d1f)/[10s7p4d1f] basis set[52−54] denoted as 6-311+G* in G98, was used throughout this work, excluding a calibration calculation on Fe_2 which was performed with the recently developed[55] correlation consistent Fe basis set. Six exchange-correlation potentials were tested, namely the combination of Becke's exchange[56] and Perdew−Wang's correlation[57] (BPW91), the exchange component of Perdew−Wang's functional[57,58] and Perdew−Wang's correlation[57] (PW91PW91), Becke's exchange[56] and Lee−Yang−Parr's correlation[59] (BLYP), Becke's exchange[56] and Perdew's correlation[60] (BP86), Becke's exchange[56] and Perdew−Burke−Ernzerhof's correlation[61] (BPBE), and, finally, Perdew−Burke−Ernzerhof's exchange and correlation (PBEPBE). The geometry was optimized for each possible spin multiplicity until further increasing the spin multiplicity would result in a state whose total energy was above the energy of the lowest asymptote. A useful empirical criterion[29,62] indicating that one has obtained the ground state is that the spin multiplicities of a neutral and its ions differ by ± 1. This "±1-rule" corresponds to an assumption that attachment and detachment of an electron are one-electron processes.

We identify the spatial symmetry of the wave function using the Slater determinant based on Kohn−Sham orbitals as is done in a conventional unrestricted Hartree−Fock scheme. For some states, whose one-electron π orbitals have not been resolved by symmetry, their assignment as Π states was supported by the results of population analyses performed within the conventional Mulliken[63] or natural atomic orbitals (NAO)[64,65] schemes. The spin multiplicity is taken to be $2 \times (n_\alpha - n_\beta)+1$.

As has been discussed previously for Cr_2, it is possible to obtain a lower energy by reducing the symmetry from $D_{\infty h}$ to $C_{\infty v}$. This corresponds to a rather spin contaminated solution. For the dimer, it is possible to make an approximate correction for this contamination,[66] but it is not clear how to proceed for larger clusters. Since the spin polarized results are in better agreement with experiment, we use this approach in this work. We do not attempt any corrections, since we are interested in the accuracy of approaches that can be easily applied to larger clusters of metal atoms. We should note that it is not always easy to obtain the spin polarized solutions and the best approach that we have found is an approach similar to that used in a search of ground states of 3d metal atoms.[67] Namely, two He atoms were placed along the Cr−Cr axis at the distances of 95 Å and 100 Å outward from chromium atoms. This lowers the symmetry to $C_{\infty v}$. The guess orbitals are taken from a calculation on the He−Cr−Mn−He doublet [at R(Mn−Cr) = 2.4 Å]. This solution is found to be antiferrimagnetic with net spins +5.5 (Cr) and −4.5 (Mn) in agreement with the previous results obtained by Desmarais et al.[30]

Since the ground states of the neutral 3d metal dimers Mn_2 and Ni_2 have not unambiguously been identified,[2−4] we paid special attention to these dimers; however, the main effort was focused on the search for the ground states of the positively and negatively singly charged dimer ions.

The zero-point energies are taken as half the computed harmonic vibrational frequencies without any scaling. The electron affinities and ionization energies reported in this work are adiabatic values; that is, each state is at its equilibrium bond length. Dissociation energies are obtained as differences in total energies of a dimer and its constituent atoms computed at the corresponding levels of theory. In the atomic computations, symmetry and equivalence restrictions are not imposed, and the solutions are in general a mixture of the $4s^23d^n$ and $4s^13d^{n+1}$ occupations.

III. Neutral Dimers

We first note that we have performed BPW91 computations on the ground $^7\Delta_u$ state of Fe_2 using both the 6-311+G* basis and the triple-ζ (TZ) correlation consistent basis set. The results obtained using the TZ basis set (r_e = 2.00 Å and ω_e = 404 cm^{-1}) are only marginally different from those obtained with the 6-311+G* basis (r_e = 2.01 Å and ω_e = 397 cm^{-1}, see Table 1). Thus we conclude that expanding the basis set will not significantly affect the results. However, as we discuss below, the results depend somewhat on the choice of the functional.

The lowest energy states of Sc_2, Ti_2, V_2, Fe_2, and Cu_2 are found to be $^5\Sigma_u^-$, $^3\Delta_g$, $^3\Sigma_g^-$, $^7\Delta_u$, and $^1\Sigma_g^+$, respectively, for all six functionals used in this work, and these are in agreement with the assignments of Hirao and co-workers[3] and Schaefer and co-workers.[4] Therefore, these dimers are not discussed in detail. For Cr_2, Mn_2, Co_2, and Ni_2, some questions arise about the ground state and/or the best theoretical approach, and therefore these states are discussed in some detail.

A. Co_2. Hirao and co-workers[3] found that their pure functionals yielded a $^5\Delta_g$ ground state of Co_2, which is in agreement with the other[68,34] calculations. They found that the hybrid B3LYP approach yielded a $^5\Sigma_g^+$ state, in agreement with configuration interaction calculations. Schaefer and co-workers reported a $^5\Sigma_g^+$ state for all the levels excluding the LSDA approach. We find a $^5\Delta_g$ ground state for all functionals considered, which is significantly below the $^5\Sigma_g^+$ state. We should note that the $^5\Delta_g$ occupation used in this work is not the same as used by Schaefer and co-workers, and this explains the different assignment despite using some of the same functionals and very similar basis sets.

B. Ni_2. In the recent DFT studies, Hirao and co-workers[3] considered only the $^3\Sigma_g^-$ and $^3\Sigma_u^+$ states of Ni_2, while Schaefer and co-workers[4] restricted their study to four singlet states. Two ab initio studies[50,69] have found the lowest state to be $^1\Gamma_g$ with five states within 0.05 eV of this state. In addition, it has been suggested[69] that after the inclusion of spin−orbit coupling, the ground state is $^1\Sigma_g^+(0_g^+)$, with only two close states.

In the first experimental study of Ni_2 by Spain and Morse,[70] the dimer was found to have a total angular momentum $\Omega = 4$, which is expected to correspond to a state that is mostly Γ in character, while their subsequent study[28] has revealed the angular moment of zero, which is expected to correspond to a $^1\Sigma$ state.

TABLE 1: Comparison of Spectroscopic Constants of the 3d Metal Dimers Obtained at the BPW91, PW91PW91, BLYP, BP86, BPBE, and PBEPBE Levels to Experiment

		Sc_2 $^5\Sigma_u^-$	Ti_2 $^3\Delta_g$	V_2 $^3\Sigma_g^-$	Cr_2 $^1\Sigma^+$	Mn_2 $^{11}\Pi_u$	Fe_2 $^7\Delta_u$	Co_2 $^5\Delta_g$	Ni_2 $^3\Sigma_g^-$	Cu_2 $^1\Sigma_g^+$	Zn_2 $^1\Sigma_g^+$
r_e/Å	BPW91	2.63	1.89	1.74	1.75	2.62	2.01	1.98	2.11	2.25	3.27
	PW91PW91	2.62	1.89	1.74	1.72	2.61	2.01	1.98	2.11	2.24	3.18
	BLYP	2.65	1.92	1.76	1.71	2.65	2.03	2.00	2.13	2.27	3.91
	BP86	2.62	1.89	1.74	1.70	2.61	2.00	1.98	2.10	2.24	3.23
	BPBE	2.63	1.89	1.74	1.75	2.61	2.01	1.98	2.11	2.25	3.24
	PBEPBE	2.63	1.90	1.74	1.72	2.62	2.01	1.98	2.11	2.25	3.21
	expt	...	1.9429 $\pm$0.0013[a]	1.77[b]	1.6788[c]	$\leq$3.4[d]	2.02 $\pm$0.02[e]	...	2.1545 $\pm$0.0004[f]	2.2193[g]	2.35 $\pm$0.08[h]
ω_e/cm^{-1}	BPW91	241	465	652	283	202	397	382	325	256	35
	PW91PW91	243	470	653	345	204	400	386	329	260	55
	BLYP	234	450	635	405	194	387	374	315	244	19
	BP86	242	470	654	400	203	402	386	330	260	52
	BPBE	241	467	652	289	203	397	383	326	257	50
	PBEPBE	243	462	651	347	203	397	381	325	257	54
	expt	238.9[i]	407.9[j]	537.5[k]	480.6 $\pm$0.5[l]	...	299.7[m]	296.8 $\pm$0.5[n]	259.2 $\pm$3[o]	266.46[p]	80 $\pm$1[q]
D_o/eV	BPW91	1.51	2.54	2.80	1.05	1.15	2.18	2.24	2.50	1.94	0.02
	PW91PW91	1.63	2.94	3.24	1.48	1.15	2.45	2.49	2.69	2.09	0.08
	BLYP	1.15	2.97	3.49	1.92	0.65	2.28	2.33	2.53	1.99	0.01
	BP86	1.51	3.00	3.39	1.69	1.05	2.36	2.42	2.64	2.05	0.04
	BPBE	1.53	2.55	2.80	1.04	1.12	2.19	2.25	2.51	1.94	0.02
	PBEPBE	1.61	2.92	3.23	1.42	1.05	2.44	2.51	2.69	2.09	0.07
	expt	1.65 $\pm$0.22[r]	1.54 $\pm$0.18[s]	2.753 $\pm$0.001[t]	1.44 $\pm$0.05[u]	$\leq$0.80[v]	1.15 $\pm$0.09[w]	1.69 $\pm$0.26[x]	2.068 $\pm$0.01[y]	2.01 $\pm$0.08[z]	0.056[aa]

[a] Ref. 85,86. [b] Ref. 87. [c] Ref. 88. [d] Ref. 79. [e] Ref. 89. [f] Ref. 28. [g] Ref. 90. [h] Ref. 91. [i] Ref. 81. [j] Ref. 92. [k] Ref. 92. [l] Ref. 5. [m] Ref. 93. [n] Ref. 94. [o] Ref. 95. [p] Ref. 90. [q] Ref. 96. [r] Ref. 97. [s] Ref. 98. [t] Ref. 99. [u] Ref. 100. [v] Ref. 1. [w] Ref. 101. [x] Ref. 102. [y] Ref. 103. [z] Ref. 1. [aa] Ref. 104.

In our work, the lowest state, for all of the DFT levels used, is $^3\Sigma_g^-$ ($7\sigma_g^2\,6\sigma_u^2\,3\pi_u^4\,3\pi_g^2\,\delta_g^4\,\delta_u^4$) followed by a $^3\Delta_g$ ($3\pi_g^4\,6\sigma_u^1\,\delta_u^3$) state that is 0.05−0.06 eV above the ground state. A $^3\Gamma_u$ state ($\delta_g^3\,\delta_u^3$) is 0.57−0.63 eV above the $^3\Sigma_g^-$ state. The lowest singlet state is $^1\Delta_g$ [$6\sigma_u^1(\alpha)1\delta_u^1(\beta)$], which is 0.43 eV(BPW91) above the $^3\Sigma_g^-$ state. We were unable to converge any $^1\Sigma_g^+$ states. Ab initio calculations find a low lying $^3\Sigma_g^-$ state with two open shell δ orbitals, while the DFT calculations yield two open-shell π orbitals. Despite these differences, the DFT spectroscopic constants are in reasonable agreement with experiment.

C. Cr_2, An Antiferromagnetic Singlet. There is a general consensus that the ground state of Cr_2 is $^1\Sigma_g^+$, even though many methods yield computed spectroscopic constants that do not agree with experiment, and the results strongly depend on the method and basis set used.[71,72] It is customary to state that the ground state of Cr_2 is antiferromagnetic. Some studies have used a symmetry-broken approach to better describe the antiferromagnetic character; two have presented the values of excess spin densities (or net spins) on chromium atoms, which are $\pm$2.54 (LSDA), $\pm$3.77 (BLYP), and $\pm$4.03 (B3P86) as found by Edgecombe and Becke[66] and $\pm$2.80 (LSDA) and $\pm$4.40 (PBEPBE) as found by Desmarais et al.[30]

For some DFT functionals,[73] the r_e and ω_e values obtained using symmetry-broken singlet of Cr_2, agree with experiment about as well as those obtained using a multiconfigurational perturbation theory approach[74] or using the most ambitious multireference configuration interaction calculations,[75] where the limit of one billion configurations was passed. Our broken-symmetry BPW91/6-311+G* calculations predict a somewhat larger bond length and lower vibrational frequency than obtained experimentally, whereas the BLYP/6-311+G* approach yields better agreement with experiment, see Table 1. Such a discrepancy between the results of computations at the BPW91 and BLYP levels is rather rare and was observed before in different assignments[76,77] of the CrO^- ground state at these two levels. If the DFT calculations are performed using $D_{\infty h}$ symmetry,[72] the differences with experiment are larger than those found for the symmetry-broken approach. Thus, while it is not ideal to break the symmetry and introduce spin contamination, it appears to be a way to obtain an improved description of Cr_2 within the DFT approximation, and we assume that this will also be true of larger Cr clusters.

D. Ground State of Mn_2. Early experimental electron-spin-resonance(ESR)[78,79] and optical spectroscopy[80] studies performed under matrix isolation conditions have suggested Mn_2 to be an antiferromagnetic, weakly bound singlet. Dissociation energies of Mn_2 determined in inert matrices have shown such wide error bars that Morse[1] was forced in his review to recommend an estimate $D_0(Mn_2) \leq 0.8$ eV. The only experimental estimate[78,79] for the equilibrium bond length of Mn_2 is $r_e = 3.4$ Å. A resonance Raman study[81] performed in argon matrices assigned the Mn_2 vibrational frequency as 124.7 cm^{-1}; however, this was reassigned[82] to Mn_3 after measurements performed in krypton matrices. This latter study assigned a vibrational constant of 76.4 cm^{-1} to Mn_2. Because of the small binding energy and large bond length, it was commonly assumed that Mn_2 is a van der Waals dimer. However, the ω_e value appears large for a true vdW molecule.

According to our computations, the ground state of Mn_2 is $^{11}\Pi_u$ at all the levels applied in this work. The $^{11}\Sigma_g^+$ state is somewhat higher in total energy. This is in agreement with other recent DFT calculations.[4,30,45,83] Our computed D_0 value is also similar to previous work. Using a symmetry-broken approach, we have also found an antiferromagnetic $^1\Sigma^+$ state. Our computations, performed at the BPW91 level, yield a net spin of $\pm$4.75 at the Mn sites, a bond length of 2.68 Å, a vibrational frequency of 128 cm^{-1}, and a dissociation energy of 0.45 eV, but this singlet state is 0.60 eV above the ground state. These results are similar to those reported previously.[83]

E. Comparison with Experiment. The results of our computations for r_e, ω_e, and D_o of the ground-state M_2 dimers are compared to experimental data in Table 1. The results obtained with the Perdew's correlation functionals PW91, P86,

TABLE 2: Spectroscopic Constants of the 3d Metal Dimer Anions Obtained at the BPW91, PW91PW91, BLYP, BP86, BPBE, and PBEPBE Levels along with the Experimental Values Obtained from Photoelectron Spectra

		Sc_2^- $^4\Sigma_g^-$	Ti_2^- $^4\Delta_u$	V_2^- $^4\Sigma_u^-$	Cr_2^- $^2\Sigma^+$	Mn_2^- $^{10}\Sigma_g^-$	Fe_2^- $^8\Delta_g$	Co_2^- $^6\Delta_u$	Ni_2^- $^4\Sigma_u^-$	Cu_2^- $^2\Sigma_u^+$	Zn_2^- $^2\Sigma_g^+$
r_e /Å	BPW91	2.73	1.93	1.76	1.74	2.39	2.07	2.03	2.17	2.36	3.06
	PW91PW91	2.72	1.93	1.75	1.72	2.38	2.07	2.02	2.17	2.35	3.02
	BLYP	2.75	1.95	1.77	1.72	2.39	2.08	2.05	2.19	2.39	3.20
	BP86	2.71	1.93	1.75	1.70	2.37	2.06	2.02	2.17	2.35	3.05
	BPBE	2.73	1.93	1.75	1.74	2.39	2.07	2.03	2.17	2.35	3.05
	PBEPBE	2.72	1.93	1.75	1.72	2.39	2.07	2.03	2.17	2.35	3.03
	expt	...	...	...	1.705 $\pm$0.010[a]	...	2.10 $\pm$0.04[b]	...	2.257 $\pm$0.017[c]	2.345 $\pm$0.010[d]	...
ω_e /cm^{-1}	BPW91	218	429	615	305	247	350	347	280	208	76
	PW91PW91	219	434	618	349	250	352	350	283	204	73
	BLYP	210	416	601	380	246	345	341	271	192	61
	BP86	218	431	617	392	251	354	350	282	202	67
	BPBE	218	430	615	310	247	350	348	281	202	66
	PBEPBE	219	426	616	347	248	350	347	280	204	72
	expt	...	...	...	440 $\pm$20[a]	...	250 $\pm$20[b]	240 $\pm$15[b]	210 $\pm$25[c]	210 $\pm$15[c]	...

[a] Ref. 5. [b] Ref. 6,7. [c] Ref. 8. [d] Ref. 9.

or PBE are nearly independent of the choice of the correlation or exchange functional for the r_e and ω_e values, while the D_o values are more sensitive to the choice. The BPW91 and BPBE levels provide similar D_o values that are generally closer to experimental data than those obtained with the BP86, PW91PW91, or PBEPBE. Excluding Cr_2, the BLYP provides slightly larger bond lengths and, correspondingly, smaller vibrational frequencies, which are closer to experimental data except for Cu_2. The experimental r_e and ω_e values for Cr_2 are reasonably well reproduced at the BLYP and BP86 levels, while this state is the worst case for the BPW91 and BPBE levels. Overall, the largest discrepancy between DFT and experiment is 0.07 Å for r_e (Cr_2), 197 cm^{-1} for ω_e (Cr_2), and 1.46 eV for D_o (Ti_2).

IV. Anions

Our results for the ground states of the M_2^- anions are presented in Table 2. As is seen, the differences between spectroscopic constants computed at the various DFT levels are somewhat larger than those for the neutral dimers presented in Table 1. Excluding Sc_2^- and Mn_2^-, the anions have a spin multiplicity that is one larger than their neutral parents, since the electron attaches to an empty α spin orbital, commonly the antibonding (4s$-$4s) orbital. For Sc_2^- the antibonding (4s$-$4s) orbital is singly occupied and thus the addition of an electron to this orbital reduces the multiplicity by one. For Mn_2, the extra electron adds to the open π bonding orbital, which reduces the multiplicity by one. For Cr_2 the "antiferrimagnetic" coupling remains after the electron attachment, as shown by the net spins at Cr sites +3.6 and $-$2.6 (BPW91) and +3.1 and $-$2.1 (BLYP).

Comparison to experimental data obtained from laser detachment photoelectron spectra of Cr_2^-, Fe_2^-, Co_2^-, Ni_2^-, and Cu_2^- shows that DFT reproduces experimental spectroscopic constants with approximately the same accuracy as for the neutral dimers. Ni_2 is an exception, where the difference between experiment and theory for the anion r_e value is 0.09 Å, while the difference is smaller (only 0.04 Å) for neutral Ni_2 (compare Tables 1 and 2). The low-lying $^4\Delta_u$ state ($6\sigma_u^1\,1\delta_u^3\,7\sigma_u^1$) is a candidate for the ground state; our computed T_e values are 0.15 eV at the BPW91 level and only by 0.005 eV at the BLYP level, and the computed bond length (BPW91: r_e = 2.212 Å, ω_e = 270 cm^{-1}; BLYP: r_e = 2.218 Å, ω_e = 262 cm^{-1}) has about the same error as found for the neutral. We should also note that we have found some anion states with longer bond lengths, namely the $^4\Delta_u(7\sigma_u^1\,6\sigma_u^1\,1\delta_u^3$, r_e = 2.30 Å, ω_e = 238 cm^{-1}) and $^4\Gamma_g^-(7\sigma_u^1\,\delta_g^3\,\delta_u^3$, r_e = 2.38 Å, ω_e = 207 cm^{-1}) states; however, the computed T_e values (at the BPW91 level), are +0.42 eV and +0.58 eV, which is sufficiently large to make them unlikely candidates for the ground state. It is unclear if we failed to find the ground state of Ni_2^-, if there is another closely spaced state of Ni_2^- with the larger bond length populated under the experimental conditions, if the error in the anion results are larger than those for the neutral, or if the fit to experimental data has a larger error than expected.

V. Cations

As shown in Table 3, the ground-state spin multiplicities of all the M_2^+ cations are larger by one than those of the corresponding neutral parents except for Ti_2^+ and Mn_2^+. Our assignment is in agreement with the experimental assignment for Sc_2^+ ($^4\Sigma_g^-$ and $^4\Sigma^{-10}$), V_2^+($^4\Sigma_g^-$ and $^4\Sigma^{-11}$), and Cu_2^+, where the experimentally determined ground state[16] is also $^2\Sigma_g^+$. For Ti_2^+, the lowest state with a spin multiplicity of four is the $^4\Delta_g$ ($6\sigma_g^1\,7\sigma_g^1\,1\delta_g^1$, BPW91: r_e = 1.95 Å, ω_e = 507 cm^{-1}) state which is 0.15$-$0.25 eV above the ground $^2\Delta_g$ state. For V_2^+, the $^2\Delta_g$ (δ_g^3, r_e = 1.62 Å, ω_e = 895 cm^{-1}) state is only 0.1 eV above the ground $^4\Sigma_g^-$ state. Thus for both Ti_2 and V_2, removing an α or β electron requires similar energies.

Detachment of an extra electron from a σ orbital of Cr_2 leads to an antiferrimagnetic $^2\Sigma^+$ state of Cr_2^+ with net spins of +2.1(+1.75) and $-$3.1($-$2.75) at the two Cr sites using the BPW91(BLYP) functional. For Mn_2^+, two levels of theory predict the lowest state to be $^{12}\Sigma_g^+$, in agreement with experiment[14] and previous DFT[45,46] studies, while four other levels predict a $^{10}\Pi_u$ ground state. Clearly it is impossible to definitively determine the ground state of Mn_2^+ from the DFT calculations. Since more functionals yield a $^{10}\Pi_u$ ground state, the results for this state are presented in Tables 3 and 4. Here, we list spectroscopic constants obtained for the $^{12}\Sigma_g^+$ ($\delta_g^2\,\delta_u^2\,3\pi_u^2\,3\pi_g^2\,7\sigma_g^1\,6\sigma_u^1\,7\sigma_u^1$) state and its position with respect to the $^{10}\Pi_u$ state: BPW91 (r_e = 2.95 Å, ω_e = 149 cm^{-1}, T_e = $-$0.002 eV), BLYP (r_e = 3.00 Å, ω_e = 141 cm^{-1}, T_e = +0.28 eV), BP86 (r_e = 2.95 Å, ω_e = 150 cm^{-1}, T_e = +0.13 eV), BPBE (r_e = 2.96 Å, ω_e = 149 cm^{-1}, T_e = $-$0.01 eV), PW91PW91 (r_e = 2.95 Å, ω_e= 152 cm^{-1}, T_e = +0.10 eV), and PBEPBE (r_e = 2.95 Å, ω_e = 152 cm^{-1}, T_e = +0.07 eV). Spectroscopic

TABLE 3: Comparison of Spectroscopic Constants of the 3d Metal Dimer Cations Obtained at the Different DFT Levels with Experiment

		Sc_2^+ $^4\Sigma_g^-$	Ti_2^+ $^2\Delta_g$	V_2^+ $^4\Sigma_g^-$	Cr_2^+ $^2\Sigma^+$	Mn_2^+ $^{10}\Pi_u$	Fe_2^+ $^8\Delta_u$	Co_2^+ $^6\Gamma_g^-$	Ni_2^+ $^4\Delta_g$	Cu_2^+ $^2\Sigma_g^+$	Zn_2^+ $^2\Sigma_u^+$
r_e/Å	BPW91	2.57	1.78	1.70	1.67	2.50	2.17	2.09	2.28	2.40	2.60
	PW91PW91	2.56	1.78	1.70	1.66	2.49	2.17	2.09	2.27	2.39	2.60
	BLYP	2.58	1.80	1.72	1.66	2.52	2.20	2.11	2.30	2.42	2.66
	BP86	2.56	1.78	1.70	1.65	2.49	2.17	2.09	2.27	2.39	2.60
	BPBE	2.57	1.78	1.70	1.67	2.49	2.17	2.09	2.28	2.40	2.60
	PBEPBE	2.57	1.78	1.70	1.66	2.50	2.17	2.09	2.28	2.39	2.61
	expt			1.7347[a]					2.2225[b]		
ω_e/cm^{-1}	BPW91	269	723	715	413	246	319	342	262	201	151
	PW91PW91	269	723	719	452	247	320	344	265	205	157
	BLYP	261	688	700	471	234	307	334	248	196	137
	BP86	269	721	720	486	249	322	345	265	205	155
	BPBE	269	726	717	414	246	320	342	262	201	156
	PBEPBE	268	720	728	449	244	320	341	262	204	155
D_o/eV	BPW91	2.54	3.09	3.51	1.30	1.91	3.35	2.97	2.87	2.02	1.73
	PW91PW91	2.79	3.46	3.91	1.69	2.10	3.57	3.21	3.13	2.14	1.85
	BLYP	2.52	3.35	3.96	2.02	2.04	3.38	3.12	2.92	2.07	1.72
	BP86	2.66	3.50	4.00	1.88	2.07	3.46	3.12	2.96	2.09	1.79
	BPBE	2.55	3.10	3.51	1.28	1.91	3.35	2.97	2.87	2.02	1.73
	PBEPBE	2.78	3.42	3.87	1.63	2.00	3.58	3.26	3.12	2.14	1.78
	expt		2.37	3.13	1.30	2.1	2.66	2.765	2.245	2.078	0.56
			±0.07[c]	±0.14[d]	±0.06[e]	±0.3[f]	±0.13[g]	±0.001[h]	±0.025[i]	±0.025[j]	±0.2[k]

[a] Ref. 12. [b] Ref. 13. [c] Ref. 20. [d] Ref. 21. [e] Ref. 22. [f] Ref. 22. [g] Ref. 24. [h] Ref. 25. [i] Ref. 28. [j] Ref. 26.

TABLE 4: Valence Electronic Configurations of the Ground State 3d Metal Dimers and Orbitals Involved in Attachment and Detachment of an Electron

species	state	neutral M_2	$+e \rightarrow M_2^-$	state	$-e \rightarrow M_2^+$	state
Sc_2	$^5\Sigma_u^-$	$6\sigma_g^2\,3\pi_u^2\,7\sigma_g^1\,6\sigma_u^1$	$6\sigma_u$	$^4\Sigma_g^-$	$6\sigma_u$	$^4\Sigma_g^-$
Ti_2	$^3\Delta_g$	$6\sigma_g^2\,3\pi_u^4\,7\sigma_g^1\,\delta_g^1$	$6\sigma_u$	$^4\Delta_u$	$7\sigma_g$	$^2\Delta_g$
V_2	$^3\Sigma_g^-$	$6\sigma_g^2\,3\pi_u^4\,7\sigma_g^2\,\delta_g^2$	$6\sigma_u$	$^4\Sigma_u^-$	$7\sigma_g$	$^4\Sigma_g^-$
Cr_2	$^1\Sigma^+$	$13\sigma^2\,5\pi^4\,14\sigma^2\delta^4$	15σ	$^2\Sigma^+$	14σ	$^2\Sigma^+$
Mn_2	$^{11}\Pi_u$	$6\sigma_g^2\,\delta_g^2\,\delta_u^2\,3\pi_u^3\,3\pi_g^2\,7\sigma_g^1\,6\sigma_u^1\,7\sigma_u^1$	$3\pi_u$	$^{10}\Sigma_g^-$	$7\sigma_u$	$^{10}\Pi_u$
Fe_2	$^7\Delta_u$	$6\sigma_g^2\,3\pi_u^4\,7\sigma_g^2\,\delta_g^3\,\delta_u^2\,3\pi_g^2\,6\sigma_u^1$	$7\sigma_u$	$^8\Delta_g$	$7\sigma_g$	$^8\Delta_u$
Co_2	$^5\Delta_g$	$6\sigma_g^2\,3\pi_u^4\,7\sigma_g^2\,\delta_g^4\,\delta_u^3\,3\pi_g^2\,6\sigma_u^1$	$7\sigma_u$	$^6\Delta_u$	$1\delta_g$	$^6\Gamma_g$
Ni_2	$^3\Sigma_g^-$	$6\sigma_g^2\,3\pi_u^4\,7\sigma_g^2\,\delta_g^4\,\delta_u^4\,3\pi_g^2\,6\sigma_u^2$	$7\sigma_u$	$^4\Sigma_u^-$	$1\delta_u$[a]	$^4\Delta_u$
Cu_2	$^1\Sigma_g^+$	$6\sigma_g^2\,3\pi_u^4\,7\sigma_g^2\,\delta_g^4\,\delta_u^4\,3\pi_g^4\,6\sigma_u^2$	$7\sigma_u$	$^2\Sigma_u^+$	$7\sigma_g$	$^2\Sigma_g^+$
Zn_2	$^1\Sigma_g^+$	$3\pi_u^4\,7\sigma_g^2\,\delta_g^4\,\delta_u^4\,3\pi_g^4\,7\sigma_u^2$	...	...	$7\sigma_u$	$^2\Sigma_u^+$

[a] The lowest energy state of Ni_2^+ is $^4\Delta_g$ ($7\sigma_g^1\,6\sigma_u^1\,\delta_u^3$).

constants of the $^{12}\Sigma_g^+$ state obtained at different levels are consistent with each other and are quite different from those obtained for the $^{10}\Pi_u$ state: bond lengths are longer by 0.45−0.50 Å and vibrational frequencies are smaller by about 100 cm^{-1}. Spectroscopic experimental data are highly desirable to resolve which is the ground state of Mn_2^+. Finally we note that there is a low-lying $^{10}\Sigma_u^+$ ($\delta_g^2\,\delta_u^2\,3\pi_u^2\,3\pi_g^2\,6\sigma_u^1\,7\sigma_g^2$) state which has a T_e value of about 0.3 eV at all the levels.

Spatial symmetry of Fe_2^+ and Cu_2^+ is defined by detachment of an electron from the β-$7\sigma_g$ orbital while the electron detaches from $7\sigma_u$ in Zn_2 to form its $^2\Sigma_g^+$ ground state. In Co_2, the electron detaches from a δ_g orbital that results in a $^6\Gamma_g$ state. The ground state of Ni_2^+ is $^4\Delta_g$ ($7\sigma_g^1\,6\sigma_u^1\,\delta_u^3$) which is not connected to the ground state of Ni_2 by a one-electron process. From the one-electron process view, this state may correspond to the $^3\Delta_g$ state of Ni_2 which is only marginally above the ground $^3\Sigma_g^-$ state. The lowest states of Ni_2^+ corresponding to one-electron detachment from the neutral ground $^3\Sigma_g^-$ state are $^4\Delta_u$ (detachment from β-δ_u) and $^4\Sigma_g^-$ (detachment from β-$7\sigma_g$). The $^4\Delta_u$ state is only marginally (0.03−0.05 eV) above the ground state, while the $^4\Sigma_g^-$ state is about 0.20 eV higher. Clearly the energy difference between the $^4\Delta_g$ and $^4\Delta_u$ states is too small to make a definitive prediction of the ground state; therefore, further studies on Ni_2 and its cation are highly desirable.

VI. Electronic Configurations

As is seen from Table 4, there is a remarkably general trend of attaching an extra electron to a σ_u orbital (except Mn_2) in order to form the anion ground state. This corresponds to increasing the 4s atomic state populations by one in all the anions except Mn_2^-, whose neutral parent has already three electrons occupying the Mn 4s states.

According to Table 4, in all the dimers except Co_2 and Ni_2, the electron detaches from a σ orbital that results in depleting 4s atomic states. The electron in Fe_2 leaves the $7\sigma_g$ orbital which is 99% 4s in character. However, the 4s occupation in Fe_2^+ is 1.50, which reflects a strong 4s−3d$_\sigma$ hybridization in this cation. In Co_2, the electron leaves a δ_g orbital in order to form the ground state of the Co_2^+ cation. As discussed above, the states of Ni_2 are close together and therefore it is difficult to determine the ground states of Ni_2 and Ni_2^+. Accordingly, it is impossible to determine if Ni_2^+ is formed by the loss of a σ electron, as found from most of the other systems, or the loss of a δ electron, as found in our calculations. The ground states of all of dimers, except Sc_2, Mn_2, and Zn_2 are derived from the $4s^13d^{n+1}$ occupations of the atoms. In the Sc_2 and Mn_2, promoting a 4s electron into the 3d shell is expensive (1.43 and 2.15 eV, respectively[105]); therefore, as discussed above, the ground states of these dimers are derived from the mixed, $4s^13d^{n+1}+4s^23d^n$,

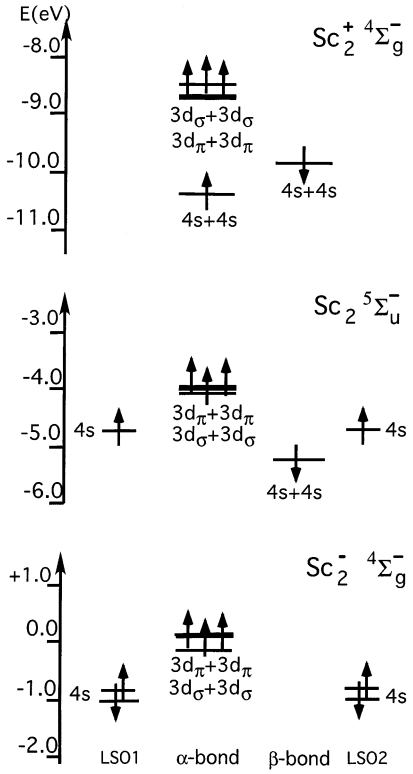

Figure 1. Bonding patterns of ground-state Sc_2, Sc_2^-, and Sc_2^+. The energy scale corresponds to orbital energies obtained using the NBO localized orbitals. The central panels present bonding orbitals (or se-bonds) in both spin representations while the left and right panels show the LSOs at the "left" and "right" atoms of a dimer. The top is for the cation, the middle for the neutral, and the bottom is for the anion.

asymptote. For Zn, the 4s to 4p promotion energy is very large and therefore the $4s^2$ Zn occupation leads to very weak (less than 0.1 eV) bonding (see Table 1).

VII. Chemical Bonding

Localized (Lewis) bonding orbitals constructed using the NBO analysis appear to be well suited for describing the chemical bonding in the 3d metal dimers, which may have occupied (neglecting small contributions from 4p and higher angular momentum orbitals) bonding 4s+4s, $4s3d_\sigma+4s3d_\sigma$, and 3d+3d orbitals and the corresponding antibonding orbitals. Since the ground states of 3d metal dimers are typically not singlets, it is appropriate to analyze the bonding separately for the spin-up (α) and spin-down (β) spin representations. We will designate the single electron bonds as se-bonds. An occupied bonding−antibonding pair in the same spin representation would appear as a pair of localized spin−orbitals (LSOs), one on each atom of the dimer. Figures 1−11 present bonding patterns obtained with the NBO analysis. Since the results, excluding Cr_2, are similar for all functionals used, we report only the results obtained with the BPW91 orbitals. For Cr_2, where the BLYP shows a somewhat different bonding pattern, we present results for the BLYP and BPW91 approaches. The energy scale corresponds to orbital energies obtained using the NBO localized orbitals[64,65] for each particular species. The central panels present bonding orbitals (or se-bonds) in both spin representations, while the left and right panels show the LSOs at the "left" and "right" atoms of a dimer and its positively (top) and negatively (bottom) charged ions.

A. Bonding Patterns in Sc_2, Sc_2^-, and Sc_2^+. Bonding patterns of these species are given in Figure 1. Due to the large $4s^23d^1 \rightarrow 4s^13d^2$ (1.43 eV[105]) promotion energy, the bonding in Sc_2 is derived from the mixed $4s^23d^1+4s^13d^2$ asymptote. The valence electronic configuration of Sc_2 is $6\sigma_g^2 3\pi_u^2 7\sigma_g^1 6\sigma_u^1$, where the β-$6\sigma_g$ orbital corresponds to a 4s+4s se-bond in the β-spin representation. The α-$6\sigma_g$ orbital combines with the α-$6\sigma_u$ orbital to produce a pair of 4s-LSOs. Two singly occupied π_u and one $7\sigma_g$ orbitals correspond to two $3d_\pi+3d_\pi$ and one $3d_\sigma+3d_\sigma$ α se-bonds. If both Sc atoms promote to $4s^13d^2$, it is possible to form three two-electron bonds: (4s+4s and a pair of $3d_\pi+3d_\pi$); this $^1\Sigma_g^+$ state is 0.35 eV above the $^5\Sigma_u^-$ ground state.[29]

To form the ground-state anion, the extra electron attaches to an antibonding β-(4s−4s) $6\sigma_u$ orbital that results in the second pair of 4s-LSOs (see Figure 1). The α-bonding orbitals of Sc_2^- are the same as in Sc_2. Note that the ground state of Sc_2^- has previously been assigned[29] as $^4\Pi_g$, which corresponds to one-electron attachment to the $3\pi_u$ orbital of the ground state.

Because of the diffuse character of valence orbitals of Sc_2 and its ions, several states with different occupation of five 3d bonding orbitals ($3d_\sigma$, $3d_\pi$, and $3d_\delta$) by three valence electrons are rather close in total energy. For example, a $^4\Delta_g$ state which corresponds to promotion of an electron from the lowest $3d_\sigma+3d_\sigma$ orbital to $3d_\delta+3d_\delta$ is only 0.17 eV(BPW91) above the ground $^5\Sigma_u^-$ state. Multireference methods would be ideal for finding all the spectrum of states of Sc_2 and its ions.

The ground-state cation arises when an electron is detached from the α-$6\sigma_u$ orbital, which destroys the two α 4s-LSOs and creates an se-bond (the $6\sigma_g$ orbital). Formation of an additional se-bond is consistent with the increased thermodynamic stability of Sc_2^+ with respect to that of Sc_2 (compare Tables 1 and 3). The NBO analysis provides a rather simple description of the bonding patterns in the series Sc_2^-, Sc_2, and Sc_2^+, which allows a qualitative understanding of bonding.

B. Bonding Patterns in Ti_2, Ti_2^-, and Ti_2^+. The $4s^23d^2 \rightarrow 4s^13d^3$ promotion energy of Ti (0.81 eV[105]) is lower than the corresponding promotion energy of Sc, and an electron is promoted to the 3d manifold on each Ti. In the ground $^3\Delta_g$ state, one two-electron 4s+4s bond, two two-electron $3d_\pi+3d_\pi$ bonds, one one-electron $3d_\sigma+3d_\sigma$, and one one-electron $3d_\delta+3d_\delta$ bond are formed. The $^1\Sigma_g^+$ state with four two-electron bonds (4s, 3dσ, and 3dπ) is higher in energy. The $^3\Delta_g$ state has the advantage of retaining some of the atomic exchange.

In the anion, the electron is added to the 4s−4s antibonding orbital, which results in an annihilation of the bonding α-(4s+4s) orbital and creates a pair of 4s LSOs. The cation is formed by detachment of a σ space α electron, which decreases the spin multiplicity by one relative to the neutral and results in bonding orbitals in both α and β spin representations that are mixtures of the 4s and 3dσ orbitals.

C. Bonding Patterns in V_2, V_2^-, and V_2^+. As in Ti_2, one 4s electron on each V is promoted into the 3d shell (promotion energy $4s^23d^2 \rightarrow 4s^13d^3$ is 0.25 eV[105]). Compared with Ti_2, the two extra electrons add to the α-$(3d_\delta+3d_\delta)$ and β-$(3d_\sigma+3d_\sigma)$ orbitals (see Figure 3), resulting in a $^3\Sigma_g^-$ ground state. All of the valence electrons in V_2 participate in chemical bonding, which makes this dimer the most stable in both the neutral and the cationic series (compare Tables 1 and 3). As found for Ti_2, the extra electron in V_2^- adds to the α-$6\sigma_u$ orbital, which annihilates the 4s+4s bond and leads to the formation of a pair of LSOs in the α space. The cation is formed by removing a σ electron from the β-spin representation, which results in a mixing of the 4s and 3dσ orbitals, thus leaving two $4s3d_\sigma+4s3d_\sigma$

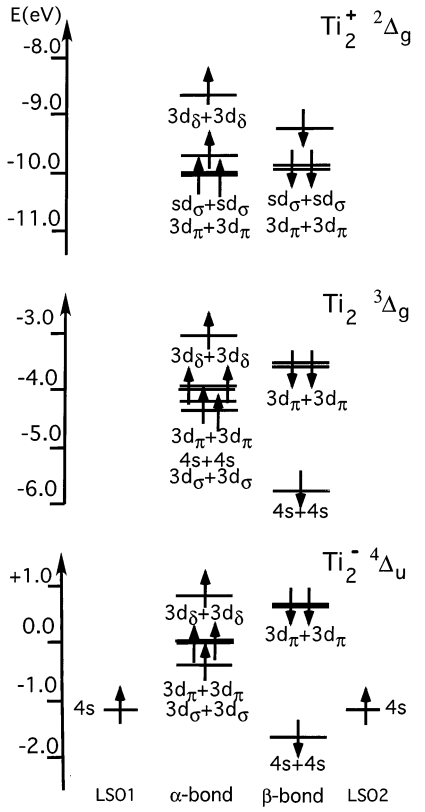

Figure 2. Bonding patterns of ground-state Ti_2, Ti_2^-, and Ti_2^+.

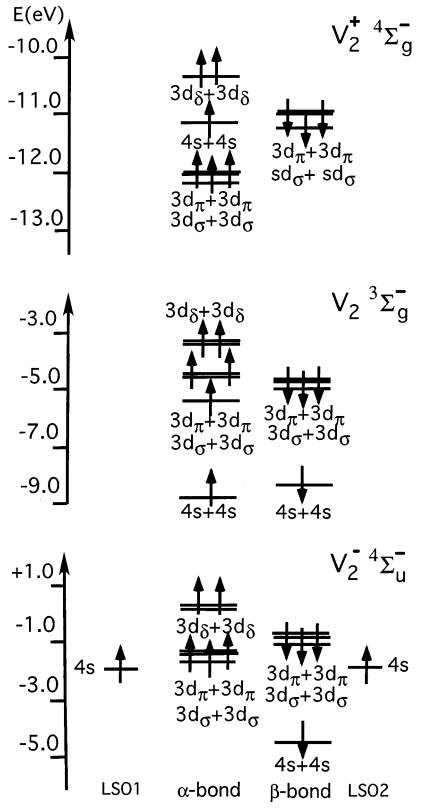

Figure 3. Bonding patterns of ground-state V_2, V_2^-, and V_2^+.

hybrid bonding orbitals in each spin representation. This is similar to the mixing observed for Ti_2^+.

D. Bonding Patterns in Cr_2, Cr_2^-, and Cr_2^+. Cr has a $4s^1$-$3d^5$ occupation and therefore, unlike Sc_2, Ti_2, and V_2, no promotion occurs. In the ground $^1\Sigma_g^+$ state of Cr_2 six bonds are

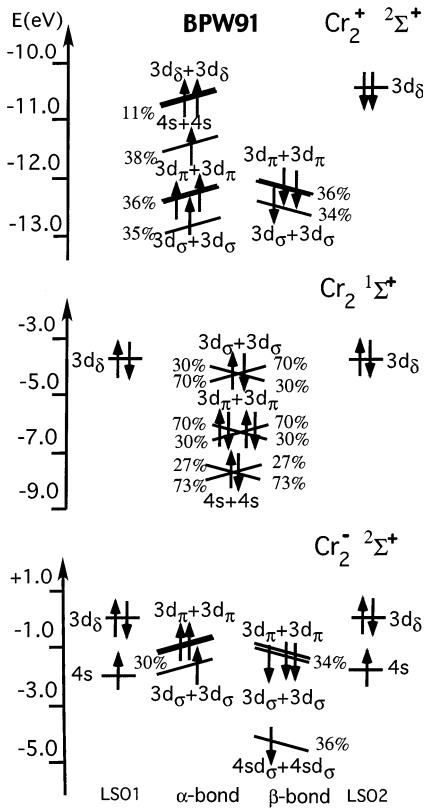

Figure 4. Bonding patterns of ground-state Cr_2, Cr_2^-, and Cr_2^+ obtained at the BPW91 level.

formed. Applying single reference methods to the $^1\Sigma_g^+$ state yields bond lengths that are too short[72] and the molecule is unstable or barely stable toward dissociation. This is due to the weak 3d−3d bonding and the large intraatomic 3d−3d exchange energy. Therefore, we prefer to lower the symmetry to $C_{\infty v}$, as described in section II, thus allowing a better description of the intraatomic 3d−3d exchange, even though this introduces some spin contamination into the approximate wave function built on the Kohn−Sham orbitals of such a symmetry-broken solution. The bonding patterns of Cr_2, Cr_2^-, and Cr_2^+ obtained using their $C_{\infty v}$ orbitals are presented in Figure 4 (BPW91) and Figure 5 (BLYP). The BPW91 (as well as the BPBE, PW91PW81, and PBEPBE) favor the formation of two $3d_\delta$ LSOs in each spin representation, while the BLYP and BP86 do not. Since the r_e and ω_e values computed at the BLYP and BP86 levels are in better agreement with experiment (see Table 1) the BLYP and BP86 bonding patterns are believed to be more representative.

As Figures 4 and 5 show, the α- and β-bonding orbitals are asymmetric. The bonding orbitals in one spin representation are polarized toward one atom, while the orbitals in the other spin representation are polarized toward the second atom. They are described by the percentage of participation of atomic orbitals near to the corresponding tilted energy level in the Figures. The BLYP α-electronic configurations at the two atoms are ($4s^{0.4}$-$3d^{1.3}$) and ($4s^{0.6}3d^{3.7}$), respectively, while the β constituents are oppositely distributed. This yields net spin densities of ±2.7 on the atoms. Localization of $3d_\delta$ orbitals at the BPW91 level increases the absolute value of the spin density at each atom, see Table 5 and Figure 4.

As in the preceding dimers, an extra electron attaches to the antibonding (4s−4s) orbital which produces an 4s LSO in each spin representation and results in the ground $^2\Sigma^+$ state of Cr_2^-. To form the ground $^2\Sigma^+$ state of Cr_2^+, the electron detaches

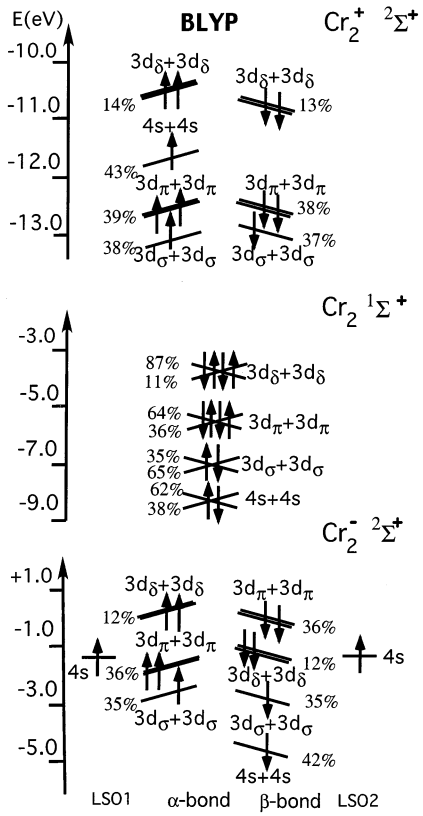

Figure 5. Bonding patterns of ground-state Cr_2, Cr_2^-, and Cr_2^+ obtained at the BLYP level.

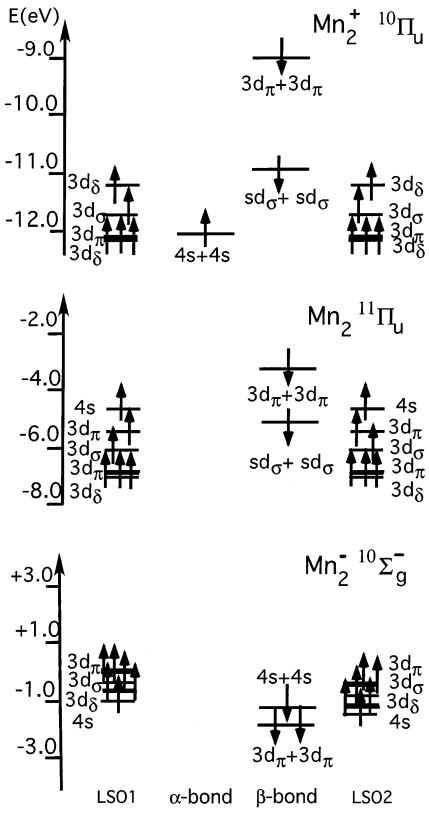

Figure 6. Bonding patterns of ground-state Mn_2, Mn_2^-, and Mn_2^+.

TABLE 5: Effective Electronic Configurations of Atoms in the 3d Metal Dimers and Their Ions

species	spin	neutral	anion	cation
Sc/Sc_2	α	$4s^{1.0}3d^{1.5}$	$4s^{1.0}3d^{1.5}$	$4s^{0.5}3d^{1.5}$
	β	$4s^{0.5}3d^{0.0}$	$4s^{1.0}3d^{0.0}$	$4s^{0.5}3d^{0.0}$
Ti/Ti_2	α	$4s^{0.5}3d^{2.0}$	$4s^{1.0}3d^{2.0}$	$4s^{0.25}3d^{1.75}$
	β	$4s^{0.5}3d^{1.0}$	$4s^{0.5}3d^{1.0}$	$4s^{0.25}3d^{1.25}$
V/V_2	α	$4s^{0.5}3d^{2.5}$	$4s^{1.0}3d^{2.5}$	$4s^{0.5}3d^{2.5}$
	β	$4s^{0.5}3d^{1.5}$	$4s^{0.5}3d^{1.5}$	$4s^{0.0}3d^{1.5}$
Cr_1/Cr_2	α	$4s^{0.7}3d^{4.0}$	$4s^{1.0}3d^{3.9}$	$4s^{0.0}3d^{3.7}$
	β	$4s^{0.3}3d^{1.0}$	$4s^{0.4}3d^{1.2}$	$4s^{0.4}3d^{1.3}$
Cr_2/Cr_2	α	$4s^{0.3}3d^{1.0}$	$4s^{1.0}3d^{1.1}$	$4s^{0.0}3d^{1.2}$
	β	$4s^{0.7}3d^{4.0}$	$4s^{0.6}3d^{3.8}$	$4s^{0.6}3d^{3.7}$
Mn/Mn_2	α	$4s^{1.0}3d^{5.0}$	$4s^{1.0}3d^{5.0}$	$4s^{0.5}3d^{5.0}$
	β	$4s^{0.5}3d^{0.5}$	$4s^{0.5}3d^{0.9}4p^{0.2}$	$4s^{0.4}3d^{0.6}$
Fe/Fe_2	α	$4s^{0.5}3d^{5.0}$	$4s^{1.0}3d^{5.0}$	$4s^{0.5}3d^{5.0}$
	β	$4s^{0.5}3d^{2.0}$	$4s^{0.5}3d^{2.0}$	$4s^{0.25}3d^{1.75}$
Co/Co_2	α	$4s^{0.5}3d^{5.0}$	$4s^{1.0}3d^{5.0}$	$4s^{0.5}3d^{5.0}$
	β	$4s^{0.5}3d^{3.0}$	$4s^{0.5}3d^{3.0}$	$4s^{0.5}3d^{2.5}$
Ni/Ni_2	α	$4s^{0.5}3d^{5.0}$	$4s^{1.0}3d^{5.0}$	$4s^{0.5}3d^{5.0}$
	β	$4s^{0.5}3d^{4.0}$	$4s^{0.5}3d^{4.0}$	$4s^{0.2}3d^{3.8a}$
Cu/Cu_2	α	$4s^{0.5}3d^{5.0}$	$4s^{1.0}3d^{5.0}$	$4s^{0.5}3d^{5.0}$
	β	$4s^{0.5}3d^{5.0}$	$4s^{0.5}3d^{5.0}$	$4s^{0.0}3d^{5.0}$
Zn/Zn_2	α	$4s^{1.0}3d^{5.0}$	...	$4s^{1.0}3d^{5.0}$
	β	$4s^{1.0}3d^{5.0}$	...	$4s^{0.5}3d^{5.0}$

[a] Corresponds to the lowest energy state of Ni_2^+ ($^4\Delta_g$).

from a 4s+4s bonding orbital. However, the asymmetry in the orbitals results in an asymmetric net spin density as found previously in the spin-broken calculations of Desmarais et al.[30] In Cr_2^-, the net spins on atoms (given by a pair of numbers in brackets) are as follows: BPW91 [+3.6, −2.6], BLYP [+3.1, −2.1], BP86 [+3.1, −2.1], BPBE [+3.6, −2.6], PW91PW91 [+3.4, −2.4], PBEPBE [+3.4, −2.4]. In the cation, the net spins on atoms are BPW91 [+3.1, −2.1], BLYP [+2.8, −1.8], BP86 [+2.8, −1.8], BPBE [+3.1, −2.1], PW91PW91 [+2.9, −1.9], PBEPBE [+3.0, −2.0].

E. Bonding Patterns in Mn_2, Mn_2^-, and Mn_2^+. Since the $4s^23d^5 \rightarrow 4s^13d^6$ promotion energy in Mn atom is the largest in the 3d metal atoms, 2.15 eV,[105] only one 4s electron is promoted into the 3d manifold of Mn_2. As in Sc_2, this results in two α-4s LSOs. The promoted electron can fill either a β-($3d_\sigma+3d_\sigma$) or a β-($3d_\pi+3d_\pi$) bonding orbital. The former leads to a $^{11}\Sigma_g^+$ state and the latter corresponds to a $^{11}\Pi_u$ state (see Figure 6). At all the levels applied here, the $^{11}\Pi_u$ state is 0.06 to 0.18 eV below the $^{11}\Sigma_g^+$ state. Note that the β-(4s+4s) orbital in the $^{11}\Pi_u$ state is better described as a $4s3d_\sigma+4s3d_\sigma$ orbital since it contains 20% of the $3d_\sigma$ AOs, while both bonding orbitals in the $^{11}\Sigma_g^+$ state are almost pure 4s+4s and $3d_\sigma+3d_\sigma$ orbitals.

There are no orbitals available for electron attachment in the α-spin representation, therefore, the extra electron may attach to a β-($3d_\sigma+3d_\sigma$) orbital (to form a $^{10}\Pi_u$ state) or to the second β-($3d_\pi+3d_\pi$) orbital (to form a $^{10}\Sigma_g^-$ state). The $^{10}\Sigma_g^-$ state is found to be somewhat lower than the $^{10}\Pi_u$ state (by 0.22 and 0.15 eV at the BPW91 and BLYP levels, respectively).

There are two options for an electron detachment: either to remove an electron from the α-4s LSO, with subsequent formation of the α-(4s+4s) bonding orbital (a $^{10}\Pi_u$ state), or to remove the electron from the β-($3d_\pi+3d_\pi$) orbital, which leaves the only one bonding orbital that is composed of half 4s and half $3d_\sigma$ atomic orbitals (a $^{12}\Sigma_g^+$ state). The $^{12}\Sigma_g^+$ state was found to be the ground state in experimental[14] and previous theoretical studies.[45−47] However, only the BPW91 and BPBE levels favor the $^{12}\Sigma_g^+$ state as the ground state of Mn_2^+, which only 0.01 eV below the $^{10}\Pi_u$ at these levels. The closeness in total energy of these two states, despite the fact that there are three bonds in the $^{10}\Pi_u$ state and only a single bond in the $^{12}\Sigma_g^+$ state, arises from the 4s→3d promotion energy needed to form the $^{10}\Pi_u$ state, while the $^{12}\Sigma_g^+$ state is formed from the atomic ground states.

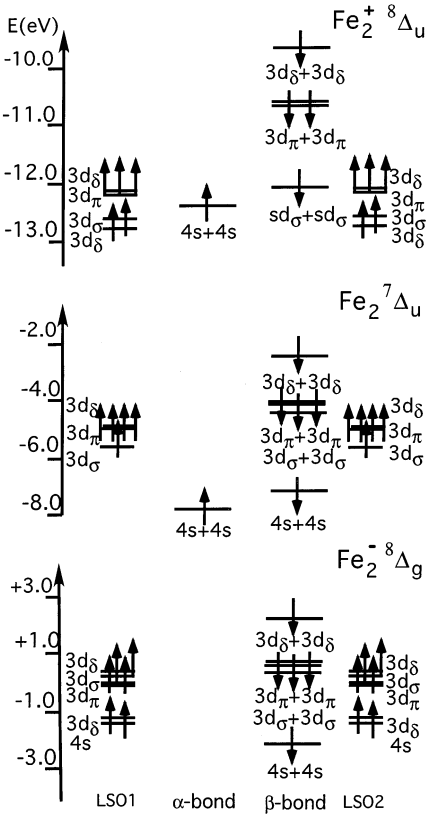

Figure 7. Bonding patterns of ground-state Fe_2, Fe_2^-, and Fe_2^+.

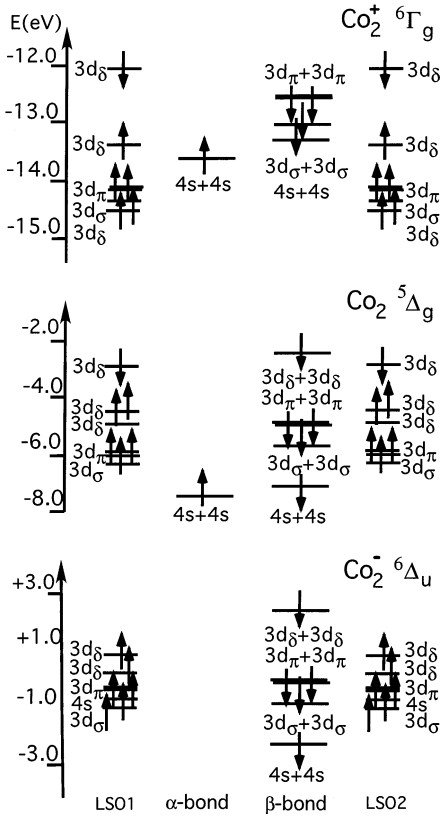

Figure 8. Bonding patterns of ground-state Co_2, Co_2^-, and Co_2^+.

F. Bonding Patterns in Fe_2, Fe_2^-, and Fe_2^+. The Fe atom 4s → 3d promotion energy of 0.87 eV is much lower than in Mn, and both Fe atoms promote to the $4s^13d^7$ occupation. This gives rise to 4s+4s se-bonds in both α and β spin representations and four β-3d se-bonds (see Figure 7). The 10 α-3d electrons occupy 10 α-3d LSOs and are chemically inert. This bonding mechanism yields a $^7\Delta_u$ ground state. Clearly, the bonding in Fe_2 is dramatically different than in Mn_2.

The most recent MRCI studies[40,41] yield a $^9\Sigma_g^-$ ground state, which is derived from the mixed $4s^13d^7+4s^23d^6$ asymptote. The bonding pattern of this state is the same as that of the Fe_2^- ground state $^8\Delta_g$ shown in Figure 7, except the $3d_\delta+3d_\delta$ orbital is empty. However, this assignment contradicts the failure[106] to observe Fe_2 in electron-spin resonance (ESR) experiments, which led to the conclusion that Fe_2 has an orbitally degenerate ground state. The $^9\Sigma_g^-$ state was found in our calculations to be above the ground $^8\Delta_u$ state by +0.51 eV and +0.64 eV at the BPW91 and BLYP levels, respectively. Attachment of an extra electron to the α- or β-(4s−4s) antibonding orbitals leads to $^8\Delta_g$ (the ground state, Figure 7) or $^6\Delta_g$, which is above the $^8\Delta_g$ state by +0.41 eV (BPW91) and +0.26 eV (BLYP).

Detachment of an extra electron from an α-4s LSO of Fe_2^- ($^8\Delta_g$) leads to formation of the ground $^7\Delta_u$ state of Fe_2, while detachment from the β-($3d_\delta+3d_\delta$) orbital results in the $^9\Sigma_g^-$ state. The energy difference between two peaks in the photoelectron spectrum measured by Leopold and Lineberger[6] is 0.53 ± 0.003 eV, which is in good agreement with our values of +0.51 eV and +0.64 eV of the $^7\Delta_u-^9\Sigma_g^-$ separation obtained at the BPW91 and BLYP levels, respectively. However, the intensity of photodetachment of a 3d electron to form the $^9\Sigma_g^-$ state is expected to be small[6] compared with the detachment of the 4s electron, while both experimental peaks possess a similar intensity. Detachment from the β-$7\sigma_g$ orbital (which is the lowest 4s+4s bonding orbital of Fe_2^-, see Figure 7) will result in a $^9\Delta_g$ state which is +0.48 eV(BPW91) above the ground $^7\Delta_u$ state. However, this state has the bond length of 2.26 Å, while the experimental results show the two neutral states having similar bond lengths and vibrational frequencies. The second $^8\Delta_u$ state may be formed due to attachment from an α-$3d_\sigma$ LSO, but this state cannot be studied using current DFT methods. Therefore, the results of our calculations are also unable to provide a definitive assignment of the experimental PES. A discussion of Fe_2, Fe_2^-, and the photoelectron spectra, based on configuration interaction methods, has been recently published.[41]

The ground state of Fe_2^+ is $^8\Delta_u$ and it formally corresponds to detachment from the β-(4s+4s) orbital; however, in the cation, the $3d_\sigma+3d_\sigma$ orbital becomes strongly 4s-hybridized (roughly 50:50).

G. Bonding Patterns in Co_2, Co_2^-, and Co_2^+. The bonding patterns of Co_2 and Co_2^- are similar to those of Fe_2 and Fe_2^-, respectively, see Figure 8. Since two extra 3d-electrons of Co_2 and Co_2^- occupy the β-$3d_\delta$ LSOs, the spin multiplicities of these species decrease by two with respect to Fe_2 and Fe_2^-, correspondingly. An electron detaches from the β-($3d_\delta+3d_\delta$) orbital of Co_2, which results in the ground $^6\Gamma_g$ state of the Co_2^+ cation. Detachment from the β-(4s+4s) orbital gives rise to a $^6\Delta_g$ state, which is somewhat higher.

H. Bonding Patterns in Ni_2, Ni_2^-, and Ni_2^+. Both additional electrons in Ni_2 must fill antibonding orbitals, which results in decreasing number of bonding orbitals and formation of the corresponding LSOs. There are three nearly degenerate states ($^3\Pi_u$, $^3\Delta_g$, and $^3\Sigma_g^-$) that correspond to different occupations of the 3d antibonding orbitals.Another series of nearly degenerate states are the singlet states which stem from formation of single 3d+3d bonds in both spin representations in addition to the two 4s+4s se-bonds. The remaining sixteen 3d-electrons form eight LSOs in each spin representation. We have optimized $^1\Delta$ and

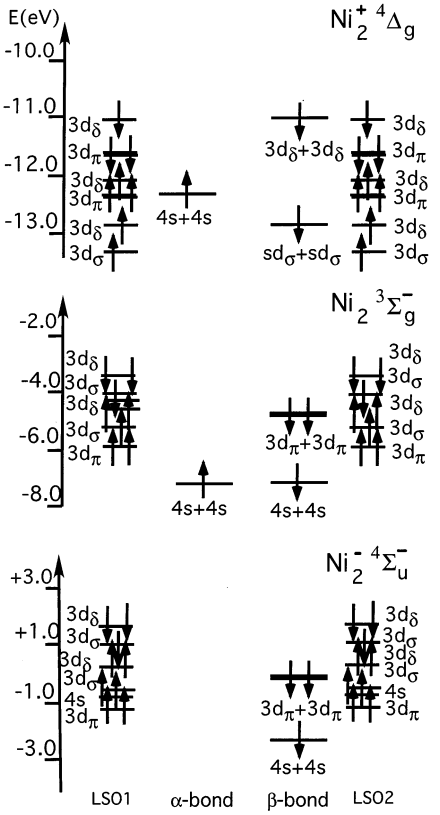

Figure 9. Bonding patterns of ground-state Ni_2, Ni_2^-, and Ni_2^+.

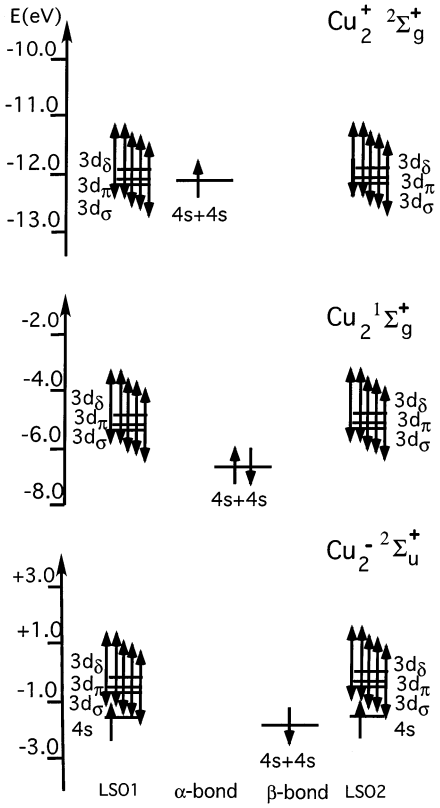

Figure 10. Bonding patterns of ground-state Cu_2, Cu_2^-, and Cu_2^+.

$^1\Pi$ states, which are above the triplet ground state by 0.35 eV (BPW91) and 0.31 eV (BLYP), respectively. We were unable to have converged any $^1\Sigma_g^+$ states.

An extra electron attaches to the α-$7\sigma_u$ (4s−4s) orbital which results in the $^4\Sigma_u^-$ state. However, the lowest energy state of Ni_2^+ found is $^4\Delta_g$, which formally has a neutral $^3\Delta_g$ state as the parent, if one assumes the ±1 rule to be valid. However, the energy differences between several states of each Ni_2, Ni_2^-, and Ni_2^+ are too small to draw definite conclusion on their ground states.

I. Bonding Patterns in Cu_2, Cu_2^-, and Cu_2^+. Copper has a $4s^13d^{10}$ electronic configuration, thus, only a 4s+4s covalent bond can be formed while 3d electrons occupy the closed 3d shell (see Figure 10). The extra electron attaches to a $7\sigma_u$ orbital which creates two α 4s LSOs and makes the ground state $^2\Sigma_u^+$. An electron detaches from the $7\sigma_g$ orbital which results in the $^2\Sigma_g^+$ ground state of Cu_2^+.

J. Bonding Patterns in Zn_2, Zn_2^-, and Zn_2^+. All the bonding and antibonding 4s- and 3d-derived orbitals are occupied in Zn_2. Their combinations form the corresponding LSOs, which results in no chemical bonding (see Figure 11) and only a small binding energy. There is a diffuse 5s4p+5s4p orbital which could accept an electron, but the derived anion state is not stable toward autodetachment. Removing a 4s electron leads to the formation of a single 4s+4s bond in Zn_2^+.

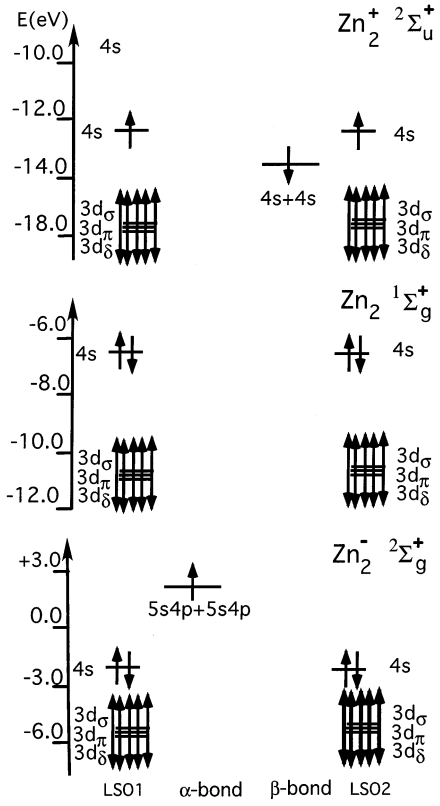

Figure 11. Bonding patterns of ground-state Zn_2, Zn_2^-, and Zn_2^+.

VIII. Electron Affinities and Ionization Energies

Adiabatic electron affinities (EA_{ad}) and ionization energies (IE_{ad}) computed as the differences in total energies of the corresponding ground states given in Tables 1−3 and described in Figures 1−11 are presented in Table 6. Zero point energies are neglected since they are smaller than 0.01 eV. As is seen from Table 6, our EA_{ad} values obtained at all the six levels are in good agreement with experiment. The BPW91, PW91PW91, BPBE, and PBEPBE levels provide values that differ by not more than 0.10 eV from each other, while the BLYP and BP86 levels provide systematically lower and higher values, respectively, with respect to the four other functionals.

TABLE 6: Adiabatic Electron Affinities and Ionization Energies of the 3d Metal Dimers

Adiabatic Electron Affinities, eV

	Sc_2	Ti_2	V_2	Cr_2	Mn_2	Fe_2	Co_2	Ni_2	Cu_2	Zn_2
BPW91	0.86	0.67	0.55	0.43	0.59	0.94	0.91	0.93	0.90	n/b[a]
PW91PW91	0.89	0.70	0.58	0.48	0.67	0.98	0.95	0.98	0.96	n/b
BLYP	0.79	0.49	0.40	0.38	0.56	0.77	0.79	0.85	0.86	n/b
BP86	0.99	0.78	0.67	0.59	0.79	1.06	1.04	1.08	1.05	n/b
BPBE	0.84	0.66	0.54	0.41	0.57	0.93	0.90	0.91	0.88	n/b
PBEPBE	0.89	0.67	0.55	0.46	0.62	0.94	0.91	0.93	0.91	n/b
expt	...	...	...	0.505 $\pm$0.005[b]	...	0.902 $\pm$0.008[c]	1.110 $\pm$0.008[d]	0.926 $\pm$0.010[e]	0.842 $\pm$0.010[f]	...

Adiabatic Ionization Energy, eV

	Sc_2	Ti_2	V_2	Cr_2	Mn_2	Fe_2	Co_2	Ni_2	Cu_2	Zn_2
BPW91	5.13	5.91	6.21	7.03	6.24	6.68	7.14	7.66	8.05	7.63
PW91PW91	5.09	5.99	6.30	7.10	6.29	6.80	7.22	7.76	8.20	7.69
BLYP	4.99	5.96	6.31	7.03	6.09	6.77	7.10	7.71	8.13	7.77
BP86	5.28	6.09	6.43	7.21	6.37	6.92	7.34	7.86	8.27	7.82
BPBE	5.12	5.89	6.19	7.01	6.22	6.66	7.11	7.63	8.03	7.59
PBEPBE	5.13	5.98	6.28	7.06	6.24	6.75	7.15	7.71	8.10	7.64
expt	...	...	6.3566 $\pm$0.0006[g]	6.9988 $\pm$0.0001[h]	$\leq$ 6.47[i]	6.30 $\pm$0.01[j]	$\leq$ 6.42[k]	7.430 $\pm$0.025[l]	7.899 $\pm$0.007[m]	9.0 $\pm$0.2[n]

[a] Indicates that Zn_2^- is not bound with respect to Zn_2+e^-. [b] Ref. 5. [c] Ref. 6. [d] Ref. 6. [e] Ref. 8. [f] Ref. 9. [g] Ref. 11. [h] Ref. 17. [i] Ref. 18. [j] Ref. 19. [k] Ref. 25. [l] Ref. 28. [m] Ref. 16. [n] Ref. 27.

The largest deviation from experiment (-0.32 eV) is obtained for the EA_{ad} of Co_2 at the BLYP level. Note that all other levels except the BP86 provide values of the Co_2 EA_{ad} that are also in the worst agreement (about -0.20 eV) with experiment. The BP86 provides the best estimate of the Co_2 EA_{ad}, which is only 0.07 eV smaller than the experimental value, but this approach provides the worst estimate ($+0.21$ eV) for the EA_{ad} of Cu_2. On the whole, agreement with experiment is rather good if one takes into account the complexity of these systems.

Experimental ionization energies are available for V_2, Cr_2, Fe_2, Ni_2, and Cu_2 with rather narrow error bars (see Table 6). Again the BPW91, PW91PW91, BPBE, and PBEPBE levels provide somewhat more consistent estimates for the experimental values. The largest deviation from the experimental values are: V_2, -0.17 eV (BPBE); Cr_2, $+0.21$ eV (BP86); Fe_2, $+0.62$ eV (BP86); Ni_2, $+0.43$ eV (BP86); Cu_2, $+0.37$ (BP86). The experimental ionization energy for Zn_2 is 1.5 eV higher than any theoretical value presented in the table, and we suspect that this experimental value is incorrect.

IX. Conclusions

According to the goals formulated in the Introduction, one may conclude the following.

(a) The BPW91, PW91PW91, BLYP, BP86, BPBE, and PBEPBE levels of DF theory provide results rather close to experiment for both spectroscopic constants and energetic properties, such as electron affinities and ionization energies, but not for dissociation energies. The results do not seem to depend on the choice of the exchange functional because BPW91 and PW91PW91 yield very similar results as do the BPBE and PBEPBE approaches. On the whole, a slight preference may be given to the BPW91 and BPBE levels, although there are marginal differences between the results obtained at these two levels and those obtained at the PW91PW91 and PBEPBE levels. The BLYP and BP86 levels provide the electron affinities and ionization energies in somewhat worse agreement with experiment.

(b) Our assignment of the neutral and cationic ground states is in good agreement with the available experimental assignments. Our assignment of the cationic and anionic ground states is consistent with the empirical "±1 rule", according to which the ground-state spin multiplicities of a species and its singly charged ions are most likely different by ±1. The most uncertain assignment is for the ground states of Ni_2 and Ni_2^+, since there are several closely spaced states in the vicinity of their ground states. Cr_2, Cr_2^-, and Cr_2^+ were studied using $C_{\infty v}$ symmetry, and all were found to possess antiferro(i)magnetic ground states, which are assigned as $^1\Sigma^+$, $^2\Sigma^+$, and $^2\Sigma^+$, respectively. The ground states of Mn_2, Mn_2^-, and Mn_2^+ are assigned as $^{11}\Pi_u$, $^{10}\Sigma_g^-$, and $^{10}\Pi_u$, respectively.

(c) The NBO analysis is well suited for description of chemical bonding patterns in the 3d metal dimers and their ions. The bonding pattern consists of localized atomic orbitals and single-electron bonds, which allows us to explain the changes in the ground-state spin multiplicities and spatial symmetries when moving along the neutral and ionic series.

(d) The ground-state multiplicity of 3d metal dimers and their ions is governed by several factors, some of which are: (i) the size of the $4s^23d^n \rightarrow 4s^13d^{n+1}$ promotion energy, (ii) the size of the 3d$-$3d intraatomic exchange energy, (iii) weakening of the 3d$-$3d bonds with increasing Z, and (iv) the preference for adding or removing electrons from the 4s orbital rather than the 3d. These factors help us explain our computed results.

Acknowledgment. G.L.G. was supported by Grants No. NCC2-5415 to University of Virginia and through contract NAS2-99092 to ELORET.

References and Notes

(1) Morse, M. D. *Chem. Rev.* **1986**, *86*, 1049.

(2) Salahub, D. R. *Ab initio methods in Quantum Chemistry$-$II*; Lawley, K. P., Ed.; Wiley: New York, 1987; pp 447$-$520.

(3) Yanasigava, S.; Tsuneda, T.; Hirao, K. *J. Chem. Phys.* **2000**, *112*, 545.

(4) Barden, C. J.; Rienstra-Kiracofe, J. C.; Schaefer, H. F., III. *J. Chem. Phys.* **2000**, *113*, 690.

(5) Casey, S. M.; Leopold, D. G. *J. Phys. Chem.* **1993**, *97*, 816.

(6) Leopold D. G.; Lineberger, W. C. *J. Chem. Phys.* **1986**, *85*, 51.

(7) Leopold, D. G.; Almlöf, J.; Lineberger, W. C.; Taylor, P. R. *J. Chem. Phys.* **1986**, *88*, 3780.

(8) Ho, J.; Polak, M. L.; Ervin, K. M.; Lineberger, W. C. *J. Chem. Phys.* **1993**, *99*, 8542.

(9) Leopold, D. G.; Ho, J.; Lineberger, W. C. *J. Chem. Phys.* **1987**, *86*, 1715.
(10) Knight, L. B.; McKinley, A. J.; Babb, R. M.; Hill, D. W.; Morse, M. D. *J. Chem. Phys.* **1993**, *99*, 7376.
(11) James, A. M.; Kowalczyk, P.; Langlois, E.; Campbell, M. D.; Ogawa, A.; Simard, B. *J. Chem. Phys.* **1994**, *101*, 4485.
(12) Yang, D. S.; Hackett, P. A. *J. Electron Spectrosc. Relat. Phenom.* **2000**, *106*, 153.
(13) Asher, R. L.; Bellert, D.; Buthelezi, T.; Brucat, P. J. *Chem. Phys. Lett.* **1994**. *224*, 525.
(14) van Zee, R. J.; Weltner, W., Jr. *J. Chem. Phys.* **1988**, *89*, 4444.
(15) Terasaki, A.; Matsushita, A.; Tono, K.; Yadav, R. T.; Briere, T. M.; Kondow, T. *J. Chem. Phys.* **2001**, *114*, 9367.
(16) Sappey, A. S.; Harrington, J. E.; Weisshaar, J. C. *J. Chem. Phys.* **1989**, *91*, 3854.
(17) Simard, B.; Lebeault-Dorget, M.-A.; Marijnissen, A.; ter Meulen, J. J. *J. Chem. Phys.* **1998**, *108*, 9668.
(18) Jarrold, M. F.; Illies, A. J.; Bowers, M. T. *J. Am. Chem. Soc.* **1985**, *107*, 7339.
(19) Rohlfing, E. A.; Cox, D. M.; Kaldor, A.; Johnson, K. H. *J. Chem. Phys.* **1984**, *81*, 3846.
(20) Lian, L.; Su, C.-X.; Armentrout, P. B. *J. Chem. Phys.* **1992**, *97*, 4084.
(21) Su, C.-X.; Hales, D. A.; Armentrout, P. B. *J. Chem. Phys.* **1993**, *99*, 6613.
(22) Su, C.-X.; Hales, D. A.; Armentrout, P. B. *Chem. Phys. Lett.* **1993**, *201*, 199.
(23) Houriet, R.; Vulpius, T. *Chem. Phys. Lett.* **1989**, *154*, 454.
(24) Markin, E. M.; Sugawara, K. *J. Phys. Chem.* **2000**, *104*, 1416.
(25) Hales, D. A.; Su, C.-X.; Lian, L.; Armentrout, P. B. *J. Chem. Phys.* **1994**, *100*, 1049.
(26) Rohlfing, E. A.; Valentini, J. J. *J. Chem. Phys.* **1986**, *84*, 6560.
(27) Buckner, S. W.; Gord, J. R.; Freiser, B. S. *J. Chem. Phys.* **1988**, *88*, 3678.
(28) Pinegar, J. C.; Langenberg, J. D.; Arrington, C. A.; Spain, E. M.; Morse, M. D. *J. Chem. Phys.* **1995**, *102*, 666.
(29) Gutsev, G. L.; Khanna, S. N.; Rao, B. K.; Jena, P. *J. Chem. Phys.* **2001**, *114*, 10738.
(30) Desmarais, N.; Reuse, F. A.; Khanna, S. N. *J. Chem. Phys.* **2000**, *112*, 5576.
(31) Castro, M.; Salahub, D. R. *Phys. Rev. B* **1994**, *49*, 11842.
(32) Hübner, O.; Sauer, J. *Phys. Chem. Chem. Phys.* **2002**, *4*, 5234.
(33) Chrétien, S.; Salahub, D. R. *Phys. Rev. B* **2002**, *66*, 155425.
(34) Gutsev, G. L.; Rao, B. K.; Jena, P. *Chem. Phys. Lett.* **2001**, *345*, 481.
(35) Weber, S. E.; Jena, P. *Chem. Phys. Lett.* **1997**, *281*, 401.
(36) Cisneros, G. A.; Castro, M.; Salahub, D. R. *Int. J. Quantum Chem.* **1999**, *75*, 847.
(37) Geskin, V. M.; Lazzaroni, R.; Mertens, M.; Jérôme, R. J.; Brédas, J. L. *J. Chem. Phys.* **1996**, *105*, 3278.
(38) Calaminici, P.; Köster, A. M.; Russo, N.; Salahub, D. R. *J. Chem. Phys.* **1995**, *105*, 9548.
(39) Tomonari, M.; Takewaki, *J. Chem. Phys.* **1988**, *88*, 1828.
(40) Hübner, O.; Sauer, J. *Chem. Phys. Lett.* **2002**, *358*, 442.
(41) Bauschlicher, C. W., Jr.; Ricca, A. *Mol. Phys.* **2003**, *101*, 93.
(42) Bauschlicher, C. W., Jr.; Langhoff, S. R.; Taylor, P. R. *J. Chem. Phys.* **1988**, *88*, 1041.
(43) Bauschlicher, C. W., Jr.; Langhoff, S. R.; Partridge, H. *J. Chem. Phys.* **1989**, *91*, 2412.
(44) Calaminici, P.; Köster, A. M.; Carrington, T., Jr.; Roy, P.-N.; Russo, N.; Salahub, D. R. *J. Chem. Phys.* **2001**, *114*, 4036.
(45) Nayak, S. K.; Jena, P. *Chem. Phys. Lett.* **1998**, *289*, 473.
(46) Terasaki, A.; Matsushita, A.; Tono, K.; Yadav, R.; Briere, T. M.; Kondow, T. *J. Chem. Phys.* **2001**, *114*, 9367.
(47) Bauschlicher, C. W., Jr. *Chem. Phys. Lett.* **1989**, *156*, 95.
(48) Bauschlicher, C. W., Jr.; Partridge, H.; Langhoff, S. R. *Chem. Phys. Lett.* **1992**, *195*, 360.
(49) Merchán, M.; Pou-Amérigo, R.; Roos, B. O. *Chem. Phys. Lett.* **1996**, *252*, 405.
(50) Partridge, H.; Bauschlicher, C. W., Jr.; Langhoff, S. R. *Chem. Phys. Lett.* **1990**, *175*, 531.
(51) Frisch, M. J.; Trucks, G. W.; Schlegel, H. B.; Scuseria, G. E.; Robb, M. A.; Cheeseman, J. R.; Zakrzewski, V. G.; Montgomery, J. A. Jr.; Stratmann, R. E.; Burant, J. C.; Dapprich, S.; Millam, J. M.; Daniels, A. D.; Kudin, K. N.; Strain, M. C.; Farkas, O.; Tomasi, J.; Barone, V.; Cossi, M.; Cammi, R.; Mennucci, B.; Pomelli, C.; Adamo, C.; Clifford, S.; Ochterski, J.; Petersson, G. A.; Ayala, P. Y.; Cui, Q.; Morokuma, K.; Salvador, P.; Dannenberg, J. J.; Malick, D. K.; Rabuck, A. D.; Raghavachari, K.; Foresman, J. B.; Cioslowski, J.; Ortiz, J. V.; Baboul, A. G.; Stefanov, B. B.; Liu, G.; Liashenko, A.; Piskorz, P.; Komaromi, I.; Gomperts, R.; Martin, R. L.; Fox, D. J.; Keith, T.; Al-Laham, M. A.; Peng, C. Y.; Nanayakkara, A.; Challacombe, M.; Gill, P. M. W.; Johnson, B.; Chen, W.; Wong, M. W.; Andres, J. L.; Gonzalez, C.; Head-Gordon, M.; Replogle, E. S.; Pople, J. A. *Gaussian 98*, rev. A.11; Gaussian, Inc.: Pittsburgh, PA, 2001.
(52) Wachters, A. J. H. *J. Chem. Phys.* **1970**, *52*, 1033.
(53) Hay, P. J. *J. Chem. Phys.* **1977**, *66*, 4377.
(54) Raghavachari, K.; Trucks, G. W. *J. Chem. Phys.* **1989**, *91*, 1062.
(55) Ricca, A.; Bauschlicher, C. W., Jr. *Theor. Chem. Acc.* **2001**, *106*, 314.
(56) Becke, A. D. *Phys. Rev. A*, **1988**, *38*, 3098.
(57) Perdew, J. P.; Wang, Y. *Phys. Rev. B* **1991**, *45*, 13244.
(58) Perdew, J. P. *Electronic Structure of Solids '91*; Ziesche, P., Eschrig, H., Eds.; Academie Verlag: Berlin 1991; p 11.
(59) Lee, C.; Yang, W.; Parr, R. G. *Phys. Rev. B* **1988**, *37*, 785.
(60) Perdew, J. P. *Phys. Rev. B* **1983**, *33*, 8822.
(61) Perdew, J. P.; Burke, K.; Ernzerhof, M. *Phys. Rev. Lett.* **1996**, *77*, 3865.
(62) Gutsev, G. L.; Khanna, S. N.; Jena, P. *Phys. Rev. B* **2000**, *62*, 1604.
(63) Mulliken, R. S. *J. Chem. Phys.* **1955**, *23*, 1833, 1841, 2338, 2343.
(64) Reed, A. E.; Weinstock, R. B.; Weinhold, F. *J. Chem. Phys.* **1985**, *83*, 735.
(65) Reed, A. E.; Curtiss, L. A.; Weinhold, F. *Chem. Rev.* **1988**, *88*, 899.
(66) Edgecombe, K. E.; Becke, A. D. *Chem. Phys. Lett.* **1995**, *244*, 427.
(67) Bauschlicher, C. W., Jr.; Gutsev, G. L. *Theor. Chem. Acc.* **2002**, *108*, 27.
(68) Jamorski, C.; Martinez, A.; Castro, M.; Salahub, D. R. *Phys. Rev. B* **1997**, *55*, 10905.
(69) Pou-Amérigo, R.; Merchán, M.; Nebot-Gil, I.; Malmqvist, P.-Å.; Roos, B. O *J. Chem. Phys.* **1994**, *101*, 4893.
(70) Spain, E. M.; Morse, M. D. *J. Chem. Phys.* **1992**, *97*, 4641.
(71) Scuseria, G. E.; Schaefer, H. F., III *Chem. Phys. Lett.* **1990**, *174*, 501.
(72) Thomas, E. J., III.; Murray, J. S.; O'Connor, C. J.; Politzer, P. *J. Mol. Struct. (THEOCHEM)* **1999** *487*, 177.
(73) Patton, D. C.; Porezag, D. V.; Pederson, M. R. *Phys. Rev. B* **1997**, *55*, 7454.
(74) Roos, B. O.; Andersson, K. *Chem. Phys. Lett.* **1995**, *245*, 27.
(75) Dachsel, H.; Harrison, R. J.; Dixon, D. A. *J. Phys. Chem.* **1999**, *103*, 152.
(76) Gutsev, G. L.; Rao, B. K.; Jena, P.; Wang, X. B.; Wang, L. S. *J. Chem Phys.* **2000**, *112*, 598.
(77) Bauschlicher, C. W., Jr.; Gutsev, G. L. *J. Chem. Phys.* **2002**, *116*, 3659.
(78) van Zee, R. J.; Baumann, C. A.; Weltner, W., Jr. *J. Chem. Phys.* **1981**, *74*, 6977.
(79) Cheeseman, M.; van Zee, R. J.; Flanagan, H. L.; Weltner, W., Jr. *J. Chem. Phys.* **1990**, *92*, 1553.
(80) Rivoal, J.-C.; Emampour, J. S.; Zeringue, K. J.; Vala, M. *Chem. Phys. Lett.* **1982**, *92*, 313.
(81) Moskowits, M.; DiLella, D. P.; Limm, W. *J. Chem. Phys.* **1984**, *80*, 626.
(82) Bier, K. D.; Haslett, T. L.; Kirkwood, A. D.; Moskowits, M. *J. Chem. Phys.* **1988**, *89*, 6.
(83) Pederson, M. R.; Reuse, F.; Khanna, S. N. *Phys. Rev. B* **1998**, *58*, 5632.
(84) Michalopoulos, D. L.; Geusic, M. E.; Hansen, S. G.; Powers, D. E.; Smalley, R. E. *J. Phys. Chem.* **1982**, *86*, 3914.
(85) Doverstål, M.; Karlsson, L.; Lindgren, B.; Sassenberg, U. *Chem. Phys. Lett.* **1997**, *270*, 273.
(86) Doverstål, M.; Lindgren, B.; Sassenberg, U.; Arrington, A.; Morse, M. D. *J. Chem. Phys.* **1992**, *97*, 7087.
(87) Spain, E. M.; Behm, J. M.; Morse, M. D. *J. Chem. Phys.* **1992**, *96*, 2511.
(88) Bondybey, V. E.; English, J. H. *Chem. Phys. Lett.* **1983**, *94*, 443.
(89) Purdum, H.; Montano, P. A.; Shenoy, G. K.; Morrison, T. *Phys. Rev. B* **1982**, *25*, 4412.
(90) Ram, R. S.; Jarman, C. N.; Bernath, P. F. *J. Mol. Spectrosc.* **1992**, *156*, 468.
(91) Carlson, K. D.; Kuschnir, K. R. *J. Phys. Chem.* **1964**, *68*, 1566.
(92) Cosse, C.; Fouassier, M.; Mejean, T.; Tranwuille, M.; DiLella, D. P.; Moskowits, M. *J. Chem. Phys.* **1980**, *73*, 6076.
(93) Moskowits, M.; DiLella, D. P. *J. Chem. Phys.* **1980**, *73*, 4917.
(94) Dong, J. G.; Hu, Z. D.; Craig, R.; Lombardi, J. R. Lindsay, D. M. *J. Chem. Phys.* **1994**, *104*, 9280.
(95) Wang, H.; Haouari, H.; Craig, R.; Lombardi, J. R.; Lindsay, D. M. *J. Chem. Phys.* **1996**, *104*, 3420.
(96) Givan, A.; Loewenschuss, A. *Chem. Phys. Lett.* **1979**, *62*, 592.
(97) Gingerich, K. A. *Faraday Symp. Chem. Soc.* **1980**, *14*, 109.

(98) Russon, L. M.; Heidecke, S. A.; Birke, M. K.; Conceicao, J. Morse, M. D.; Armentrout, P. B. *J. Chem. Phys.* **1994**, *100*, 4747.
(99) Spain, E. M.; Morse, M. D. *J. Chem. Phys.* **1992**, *96*, 2479.
(100) Hilpert, K.; Ruthardt, K. *Ber. Bunsen-Ges. Phys. Chem.* **1987**, *91*, 724. Their value was recommended by Morse.[1] A recent experimental study[17] suggests $D_0(Cr_2) = 1.53 \pm 0.06$ eV.
(101) Loh, S. K.; Lian, L.; Hales, D. A.; Armentrout, P. B. *J. Phys. Chem.* **1988**, *92*, 4009.
(102) Kant, A.; Strauss, B. J. *J. Chem. Phys.* **1964**, *41*, 3806.
(103) Morse, M. D.; Hansen, G. P.; Langridge-Smith, P. R. R.; Zheng, L.-S.; Geusic, M. E.; Michalopoulos, D. L.; Smalley, R. E. *J. Chem. Phys.* **1984**, *80*, 5400.
(104) Su, C.-H.; Liao, P.-K.; Huang, Y.; Liou, S.-S.; Brebrick, R. F. *J. Chem. Phys.* **1984**, *81*, 11.
(105) Morse, M. D. *Advances in Metal and Semiconductor Clusters*; JAI Press Inc.: Greenwich, CT, 1993; Vol. 1, pp 83−121.
(106) Bauman, C. A.; van Zee, R. J.; Weltner, W. *J. Phys. Chem.* **1984**, *88*, 1815.